MONITORING OF RECENT LAND SUBSIDENCE AND GROUND FISSURES IN XIAN WITH SAR INTERFEROMETRY

Chaoying Zhao[1,2], Xiaoli Ding[1], Qin Zhang[2], Zhong Lu[3] Zhiwei Li[1]

[1] Department of Land Surveying and Geo-Informatics, The Hong Kong Polytechnic University, Hung Hom, Hong Kong, China - (zhaochaoying@163.com, lsxlding@inet.polyu.edu.hk, zwli@mail.csu.edu.cn)
[2] School of Geological Engineering and Geomatics, Chang'an University, Xian Shaanxi, China -zhangqin@263.net.cn
3 U.S. Geological Survey, Vancouver, Washington, USA - (lu@usgs.gov)

KEY WORDS: Land subsidence, Ground fissure, Differential InSAR, Monitoring

ABSTRACT:

The City of Xian, China, has been experiencing significant land subsidence and ground fissure activities since 1960s that have brought various severe geohazards including damages to buildings, bridges and other facilities. Monitoring of land subsidence and ground fissure activities can provide useful information for assessing the extent of, and mitigating such geohazards. We study the land subsidence and ground fissure activities during 1992 - 2006 using ERS and Envisat SAR data. Three main land subsidence stages in 1992, 1996 and post 2004 are identified. The maximum land subsidence rates increased from 16cm/a in 1992 to 22 cm/a in 1996 and then decreased to 7.5cm/a by 2004, while the area affected by the subsidence expanded from the first stage to the second and then decreased from the second to the third. Some of the ground fissures that were active during 1990s became inactive after 2004 while some new fissures appeared in the new subsidence areas. It is also found that the land subsidence and ground fissure activities were related to ground water withdrawal and city development.

1. BACKGROUND

Xian, the Capital City of Shaanxi Province, lies in the middle of Wei River Basin, in northwestern China. Four main rivers, Wei River, Ba River, Chan River and Zao River surround the city in the northern, eastern and western suburbs respectively (Figure 1). The Chang'an-Lintong fault (CAF hereinafter), one of the main active faults controling the geological activities of the region (Peng et al., 1992), lies in the southern side of the city. Xian has been undergoing serious land subsidence and ground fissure activities since 1960s mainly due to ground water withdrawal and the CAF (Zhang, 1990; Yi et al., 1997; Wang, 2000; Suo et al., 2005). Levelling measurements started in 1959 have shown that by earlier 1990s the areas with cumulative subsidence of more than 200 mm were over 145 km^2; the maximum subsidence was 2322 mm; the average ground subsidence rate was 50-100 mm/a; the maximum subsidence rate was up to 300 mm/a; and there existed eight subsidence funnels in the southern, eastern and southwestern suburbs of the city (Tao, 1999). The number of ground fissures has further increased since then. The ground fissures and CAF are approximately in an east-north easterly (ENE) direction, which resulted in ellipsoidal subsidence cones with their major axes being approximately parallel to the directions of the ground fissures (Lee et al.,1996; Yan, 1999; Xian City Planning Bureau, 2006). A contour map of subsidence from levelling measurements of 1959 to 1995 is shown in Figure 1 with the known ground fissures superimposed onto the map. Unfortunately, regular levelling measurements have not been conducted since 1995. Not much information is therefore available for assessing the recent ground subsidence and fissure activities.

We will in this work analyze 15 ERS 1/2 and Envisat SAR scenes to study the evolution of land subsidence during 1992 - 2007. Some GPS data will also be used to validate the InSAR results.

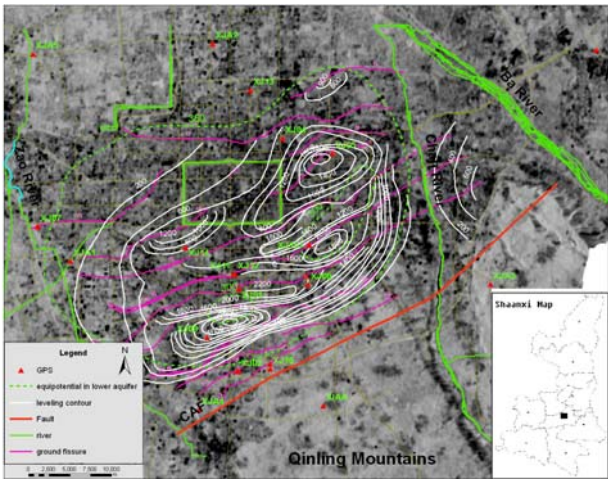

Figure 1. Location map of Xian City, where 3 rivers, the CAF, 13 ground fissures, contour map of subsidence from levelling measurements of 1959 to 1995, confined water contour and GPS stations are plotted on a SAR magnitude map. The green rectangle is the ancient Xian city wall. The inset is the map of Shaanxi Province, where the black rectangle represents the study area.

2. DATA SETS AND PROCESSING

Fifteen ERS and Envisat SAR images acquired during 1992 – 2007 (see Table 1) are selected for this study. Six interferometric pairs with time intervals from 140 to 595 days and baselines of less than 200 m (Table 2) are formed and analyzed in detail.

No.	Date of Acquisition	Sensor	Track
1	1992.09.11	ERS1	390
2	1992.09.30	ERS1	161
3	1993.01.29	ERS1	390
4	1993.02.17	ERS1	161
5	1993.03.05	ERS1	390
6	1993.04.09	ERS1	390
7	1996.01.07	ERS1	390
8	1996.07.01	ERS2	390
9	1998.05.16	ERS2	161
10	1998.06.20	ERS2	161
11	2004.01.10	Envisat	2161
12	2005.06.18	Envisat	2161
13	2005.08.27	Envisat	2161
14	2006.04.29	Envisat	2161
15	2007.03.10	Envisat	2161

Table 1. SAR data selected for the research

Pair No.	Master	Slave	$B_{\perp}$ (m)	Temporal Baseline	Sensor
1	92.09.11	93.04.09	30.4	210	ERS
2	92.09.30	93.02.17	124.1	140	ERS
3	96.01.07	96.07.01	-37.2	175	ERS
4	04.01.10	05.08.27	119.5	595	Envisat
5	05.06.18	06.04.29	27.3	315	Envisat
6	06.04.29	07.03.10	175.7	315	Envisat

Table 2. InSAR pairs formed

Two-pass differential interferometric synthetic aperture radar (DInSAR) method is applied with the 3 arc second SRTM DEM used for removing the topographic phase. The maximum elevation difference in the study area is within 100 m so that the effects of the errors in the DEM are negligible for the short normal baselines of the InSAR pairs. Precise ERS and Envisat orbit data from the Delft University are applied to mitigate the satellite orbit errors (Scharroo et al., 1998). The adaptive filtering algorithm (Li et al., 2006) is applied to reduce the phase noise in the interferograms. The minimum cost flow method is applied (Chen and Zebker, 2001) to unwrap the interferograms. The results are then geocoded and projected into the vertical direction considering the fact that the main deformation in the area is subsidence. Finally we select a square window of 20*20 pixels in a stable area to use their median value as the stable point value and then adjust the results from each InSAR pair to obtain the absolute subsidence values between the image acquisitions.

Seventeen GPS stations were set up in 2005 and two measurement campaigns were carried out on June 2005 and June 2006. The locations of the GPS stations are shown in some of the plots in Figure 2. To compare the InSAR and GPS measurement results, the subsidence values at the discrete GPS stations are extracted from the subsidence map of InSAR Pair 5 (050618-060429) and converted into annual subsidence rates. The correlation between the InSAR and GPS measurements at the GPS stations is then calculated. In addition, to depict the evolution of land subsidence over 1992 - 2007 and to detect the differential subsidence rates across the ground fissures, two profiles (see Figure 2) of subsidence, AA' that starts from the stable point (Point A) and extends to the CAF and BB' that is along one of the main streets in the city are generated and are shown in Figure 3.

3. RESULTS AND DISCUSSIONS

3.1 Results

The six geocoded subsidence maps are shown in Figure 2 with the two profiles of subsidence AA' and BB' marked on the maps. The profiles of subsidence from five of the maps are shown in Figures 3(a) and 3(b) respectively. Figure 4 gives the correlation between the GPS and InSAR results from Pairs 5.

3.2 Discussions

It can be seen that the large subsidence gradients in some of the areas (Figure 2). The overall coherence of the interferograms also varied in time with the expansion of the city areas. For example, the coherence in the northeastern and southwestern suburbs of the city was getting better as large Hi-tech zones have been gradually built up in the areas since 1996.

The accuracy of the InSAR results is assessed against the GPS results at the GPS stations. Figure 4 shows the annual subsidence rates at the GPS stations determined from the InSAR and the GPS measurements. The overall correlation between the two types of measurements is 0.725, and this increases to 0.867 if the outlying ground fissure point XJ03 is removed. Most of the residuals from the linear regression are within 1cm/a.

All the subsidence maps have shown that the northwestern part of the city was stable, while the southeastern and southwestern suburbs have been experiencing the most significant subsidence. It can also be seen that the subsidence was highly correlated to the locations and directions of the ground fissures that are mainly in the NEN direction. Some ellipsoidal subsidence cones can be identified between the fissures with their major axes being parallel to the directions of the fissures. The differential subsidence values on the two sides of the ground fissures are up to about 2 cm as seen in Figure 3.

The subsidence rate has evolved over the past 15 years as seen in Figure 2. First, both the subsidence rate and the area affected increased from 1992 to 1996. By examining the results in Figures 2(a) and 2(c), it can be seen that the maximum subsidence rate increased from 16cm/a to 20cm/a over this period of time. In the same time, the subsidence rate in the eastern suburbs also increased. These can also be seen in the subsidence profiles given in Figure 3. Second, the subsidence cones shifted to the western and southeastern parts of the city after 2004, while the northeastern part became stable after 2006. The maximum subsidence rate also slowed down to about 7.5cm/a by 2005 and 2006, as shown in Figures 2(e) and 2(f).

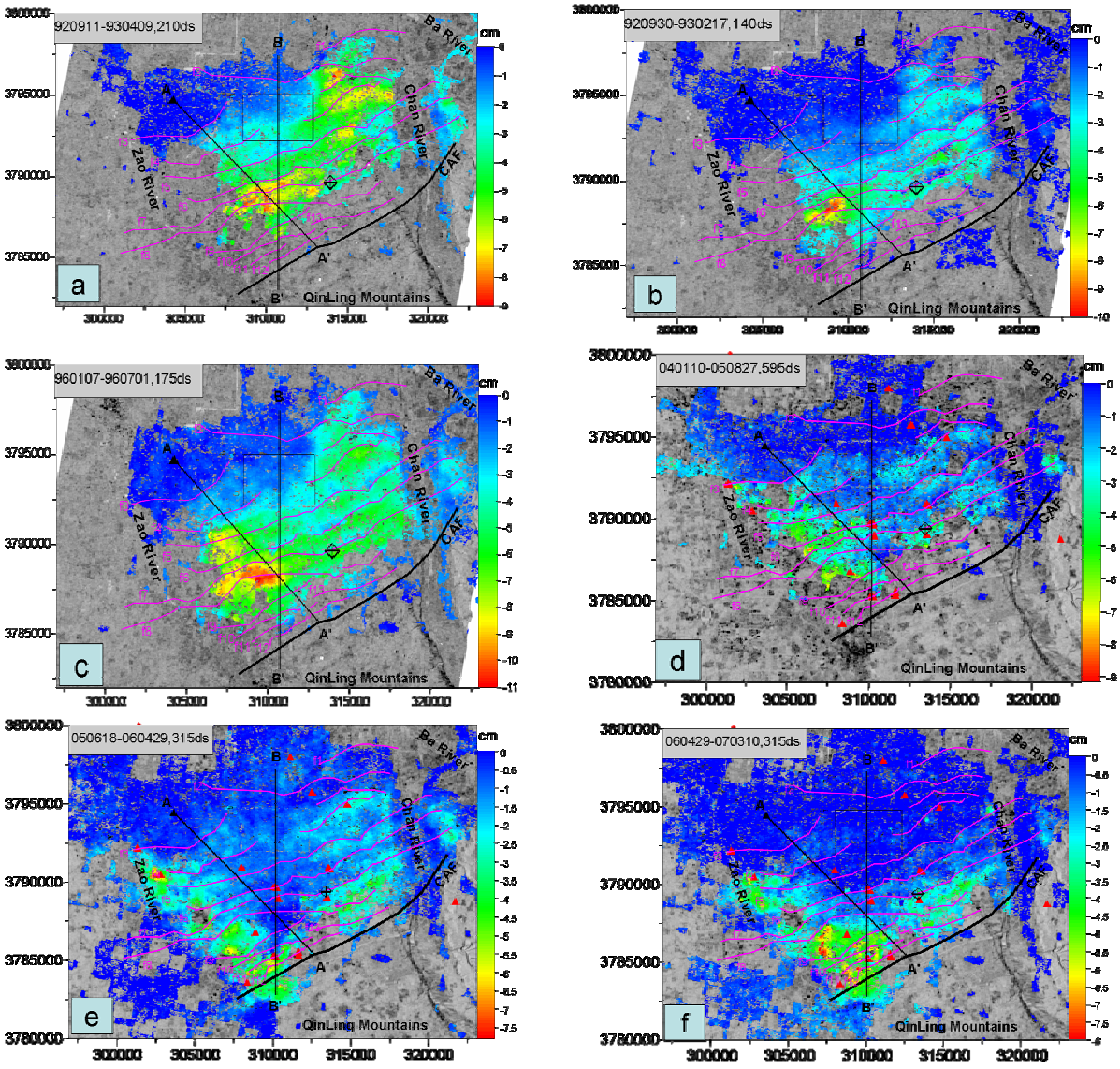

Figure 2. Subsidence maps corresponding to interferometric pairs listed in Table 2. AA' and BB' are two profiles along which the subsidence is examined in detail. The red triangles in Figures (d), (e) and (f) are GPS stations set up in 2005.

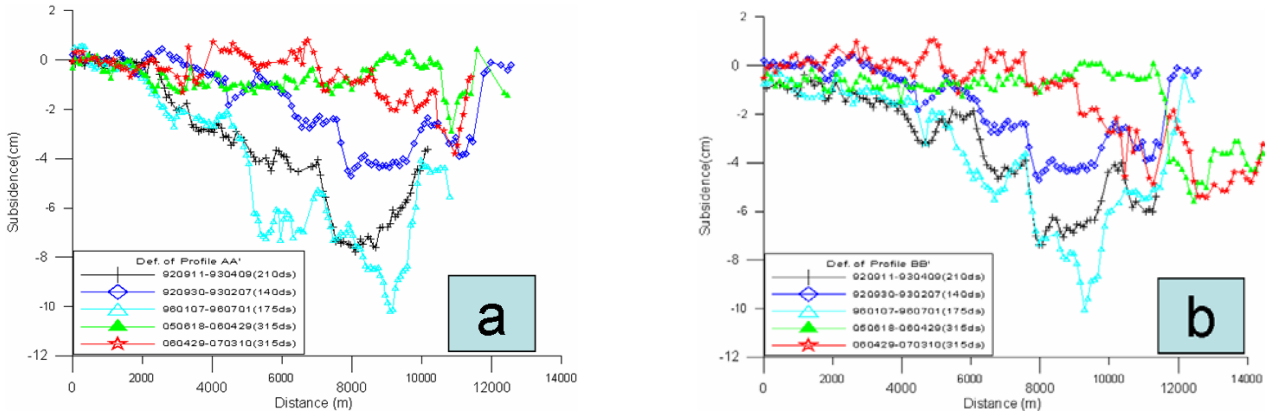

Figure 3. Subsidence along profiles AA' and BB' shown in Figure 2.

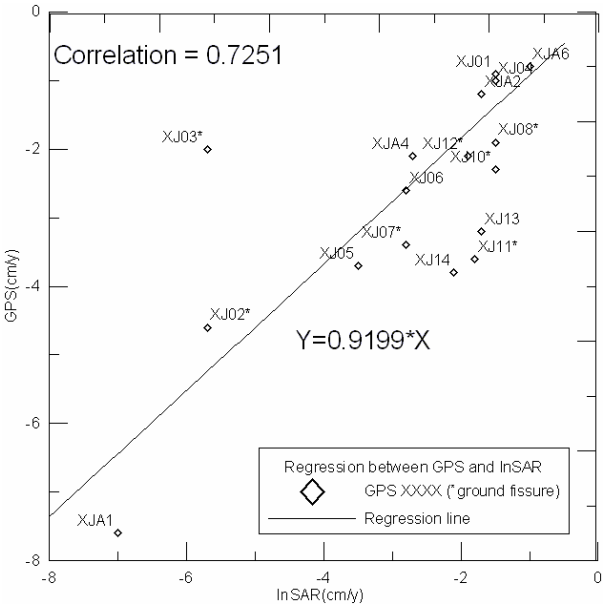

Figure 4. Correlation between annual subsidence rates determined based on GPS and InSAR measurements over 2005 - 2006. The points marked with asterisk are GPS stations set up for ground fissure monitoring.

4. CONCLUSIONS

Results from ERS and Envisat InSAR measurements over 1992 – 2007 have shown that the ground subsidence in Xian was significant over this period of time. The subsidence rate increased from 1992 to 1996, and then decreased from 1996 to 2004 and the main subsidence areas shifted to the newly developed suburbs. The subsidence was correlated spatially to the distribution of the ground fissures and the CAF, and to ground water withdrawal.

ACKNOWLEDGEMENTS

The SAR data were provided by ESA under two Category 1 projects. The research was financially supported by a Key Project of the Natural Science Foundation of China (NSFC) (Project No: 40534021), a general project of the NSFC (Project No: 40672173), a Key Project of the Ministry of Land & Resources, China (Project No: 1212010440410), and by the Research Grants Council (RGC) of the Hong Kong Special Administrative Region (Project No.: PolyU 5161/06E).

REFERENCES

Amelung, F., Galloway, D.L., Bell, J.W., Zebker, H.A. and Laczniak, R.J., 1999, Sensing the ups and downs of Las Vegas: InSAR reveals structural control of land subsidence and aquifer-system deformation, Geology, 27(6): 483-486.

Chen, C.W. and Zebker, H.A., 2001, Two-dimensional phase unwrapping with use of statistical models for cost functions in nonlinear optimization, J. Opt. Soc. Amer. A, 18:. 338–351.

Lee, C.F., Zhang, J.M. and Zhang, Y.X., 1996, Evolution and origin of the ground fissures in Xian China, Engineering Geology 43: 45-55.

Li, ZW., Ding, X.L., Huang, C., Zheng, D.W., Zou, W.B. and Shea, Y.K., 2006, Filtering Method for Radar Interferogram with Strong noise, International Journal of Remote Sensing, 27(14): 2991-3000.

Peng, J.B., Su, S.R. and Zhang, J., 1992，The Active Faults and Geohazards in Weihe Basin, Northwest university Press, Xian.

Scharroo, R., Visser, P.N.A.M., and Mets, G.J., 1998, Precise orbit determination and gravity field improvement for ERS satellites, Journal of Geophysical Research, 103(C4): 8113-8127.

Suo, C.M., Wang, D.Q., Liu, Z.Z., 2005, Land fracture and subsidence prevention in Xian, Quaternary Research, 25(1): 23-28.

Tao, H., 1999, The Land Subsidence Map of Xian City, in Xian Environmental Geological Atlas, Xian Mapping Press, Xian.

Wang, J.M., 2000, Theory of Ground Fissures Hazards and Its Applications, Shaanxi Science and Technology Press, Xian.

Xian City Planning Bureau, 2006, Regulations of Field Reconnaissance and Engineering Design of Xian Ground Fissures, Institute of Geotechnical Investigation and Design MMI and China Northwest Building Design Research Institute, Xian City Planning Bureau, No. DBJ61-6-2006.

Yan, W.Z., 1999, Xian Ground Fissures Map, in Xian Environmental Geological Atlas, Xian Mapping Press, Xian.

Yi, X.F., Su, G., Wang, W.D. and Tang, J.C., 1997, Basic characteristics of the fissure zones in Xian and their causative mechanism, Seismology and Geology, 19(4): 289-294.

Zhang, J.M., 1990, Research on Ground Fracture in the Region of Xian, Northwest University Press, Xian.